Available online at www.sciencedirect.com
ScienceDirect
Trans. Nonferrous Met. Soc. China 30(2020) 3333−3346
Transactions of Nonferrous Metals Society of China
www.tnmsc.cn

Preparation of $NaYF_4:Yb^{3+},Tm^{3+}@NaGdF_4:Ce^{3+},Eu^{3+}$ double-jacket microtubes for dual-mode fluorescent anti-counterfeiting

Yin CHEN[1], Shao-wen XIE[1], Chao TONG[1], Hai-hu TAN[1], Li-jian XU[1], Na LI[1,2], Jian-xiong XU[1]

1. Hunan Key Laboratory of Biomedical Nanomaterials and Devices, College of Life Sciences and Chemistry, Hunan University of Technology, Zhuzhou 412007, China;
2. Key Laboratory of Electrochemical Green Metallurgy Technology of Hunan Higher Education Institutions, College of Metallurgy and Materials Engineering, Hunan University of Technology, Zhuzhou 412007, China

Received 22 February 2020; accepted 4 September 2020

Abstract: Novel hydrophilic $NaYF_4:Yb^{3+},Tm^{3+}@NaGdF_4:Ce^{3+},Eu^{3+}$ double-jacket microtubes (DJMTs) with upconversion/downconversion dual-mode luminescence were designed and prepared through epitaxial growth of $NaGdF_4:Ce^{3+}$, Eu^{3+} shell onto the $NaYF_4:Yb^{3+},Tm^{3+}$ microtube via poly(acrylic acid) (PAA) mediated hydrothermal method. It is demonstrated that PAA ligand played an important role in guiding the direct growth of $NaGdF_4:Ce^{3+},Eu^{3+}$ shell onto the surface of $NaYF_4:Yb^{3+},Tm^{3+}$ parent microtubes. The growth of $NaGdF_4:Ce^{3+},Eu^{3+}$ shell experienced a crystal phase transition from β-$NaGdF_4$ and β-$NaYF_4$ mixture to β-$NaYF_4@NaGdF_4$ composite crystal, and morphology evolution from mixture of β-$NaGdF_4:Ce^{3+},Eu^{3+}$ nanorods and β-$NaYF_4:Yb^{3+},Tm^{3+}$ microtubes to $NaYF_4:Yb^{3+},Tm^{3+}@NaGdF_4:Ce^{3+},Eu^{3+}$ DJMTs. The formation mechanism of DJMTs was the dissolution−renucleation of β-$NaGdF_4:Ce^{3+},Eu^{3+}$ nanorods and the growth of β-$NaGdF_4:Ce^{3+},Eu^{3+}$ shell via the classical Ostwald ripening mechanism. The as-prepared DJMTs could exhibit blue upconversion and red downconversion luminescence, which was further made into environmentally benign luminescent inks for creating highly secured and fluorescent-based anti-counterfeiting patterns via inkjet printing.

Key words: lanthanide-doped fluoride; core−shell structure; dual-mode luminescence; inkjet printing; anti-counterfeiting

---

1 Introduction

Nowadays, counterfeit products have significant impact on the interests of consumers and cause huge business economic losses [1,2]. Developing of efficient anti-counterfeiting technology is becoming critical, aiming to distinguish forge products and protect intellectual property [3−5]. In recent decades, a variety of anti-counterfeiting products such as radio frequency identification (RFID) [6], laser holography [7], nuclear trackers [8], and luminescent materials [9−11], have been developed to combat the counterfeiting. Among them, luminescence materials and their corresponding anti-counterfeiting technologies are considered as one of the most perspective ways to boycott counterfeiting because of their diverse chemical nature, unique optical properties, and easy availability [12−15]. During the past years, some fluorescent materials including organic dye molecules [16], semi-conductor quantum dots [17], and carbon dots [18] have been developed and applied for anti-counterfeiting. However, these well-studied anti-counterfeiting technologies are relatively easy to be

---

Foundation item: Project (51874129) supported by the National Natural Science Foundation of China; Projects (2018JJ3115, 2019JJ60049) supported by the Science Foundation of Hunan Province, China; Projects (19B153, 19B158) supported by the Scientific Research Fund of Hunan Provincial Education Department, China

Corresponding author: Na LI; Tel: +86-731-28123470; E-mail: lina@hut.edu.cn

DOI: 10.1016/S1003-6326(20)65465-6

cracked by the skilled counterfeiters. Besides, the broad emission bands, low photostability and biological toxicity of these fluorescent materials are still drawbacks [19].

Recently, the lanthanide-doped fluoride luminescent ($NaREF_4$:Ln^{3+}) materials are recognized as a competitive alternative for anti-counterfeiting application due to their advantages of environmental friendship, long fluorescence life, multicolor optical properties, and sharp emission bands [20−23]. Moreover, the strong dependence of the color output on the excitation source including power density, pulse duration, and excitation wavelength offers additional benefits in fine-tuning the emission profiles, which is essential for practical applications in anti-counterfeiting and high-capacity information storage [24−27]. Due to the rich energy level pattern of lanthanides, $NaREF_4$:Ln^{3+} materials can be divided into two categories of upconversion (UC) and down-conversion (DC) depending on the luminescence mechanism [28,29]. Generally, the upconversion process can absorb low energy photons and convert them into high energy photons, while down-conversion refers to the opposite process. Typically, the efficient upconversion $NaREF_4$:Ln^{3+} materials doped with lanthanide ion pairs such as Yb^{3+}/Er^{3+} and Yb^{3+}/Tm^{3+} in $NaYF_4$ host material can harvest pumping photons and emit multiple wavelengths [23,30,31]. Similarly, downconversion $NaREF_4$:Ln^{3+} materials can also emit different colors depending on the doping category such as Tb^{3+} (green), Eu^{3+} (red), and Ce^{3+} (yellow) under short wavelength excitation [32,33].

In the past years, $NaREF_4$:Ln^{3+} luminescent materials with single color emission have been studied extensively and applied in anti-counterfeiting filed [34,35]. Nevertheless, they are still easy to duplicate owing to their simplicity. On the contrary, multi-mode luminescent materials have shown their advantages since the anti-counterfeiting technique is more complicate and difficult to simulate. Specially, dual-mode luminescent $NaREF_4$:Ln^{3+} materials that integrate UC and DC emission with different emission colors have aroused significant interests in high anti-fake level of anti-counterfeiting techniques [36−39]. Previous approach concerning dual-mode $NaREF_4$:Ln^{3+} materials is simple mixing of DC and UC $NaREF_4$:Ln^{3+} luminescent materials together to produce dual-mode luminescence [40]. However, this approach is time-consuming and process-tedious, and it is difficult to control the spatial distribution of UC and DC materials because the synthesis processes of DC and UC $NaREF_4$:Ln^{3+} luminescent materials are spatially separated. To obtain stable dual-mode $NaREF_4$:Ln^{3+} luminescent materials, promising strategy is to integrate both DC and UC materials into a single structure. For example, several studies have reported the dual-mode $NaREF_4$:Ln^{3+} luminescent materials by doping multiple UC and DC lanthanide activators into the identical matrix materials [41]. However, the cross relaxation between the rare earth ions under multiple doping conditions inevitably leads to the depression of luminescence intensity. A modified method is dividing UC and DC ions into different layers of $NaREF_4$:Ln^{3+} luminescent materials using the core−shell structure to achieve dual-mode luminescent materials [42−46]. This spatially confined structure could effectively depress the deleterious energy depletion. For example, LIU et al [43] reported a novel strategy to prepare dual-mode luminescent $NaGdF_4$ nano-crystals consisting of $NaGdF_4$:Yb,Tm core and $NaGdF_4$:Eu shell. In this core−shell structure, the $NaGdF_4$:Yb,Tm core can emit UC luminescence of Eu^{3+} in the shells by using double sensitizers (Yb^{3+} and Tm^{3+}). Meanwhile, the red DC luminescence of Eu^{3+} could be achieved under the excitation at 273 nm. DING et al [44] also synthesized dual-mode fluorescent nanocrystals by coating a $NaGdF_4$:Ce,Tb shell with DC emission on the surface of UC nanoparticles of $NaGdF_4$:Yb/Tm. Recently, our group synthesized dumbbell-shaped lanthanide-doped $NaYF_4$@$NaGdF_4$ core−shell nanoparticles with dual-mode fluorescence by coating $NaGdF_4$:Ln^{3+} shell onto $NaYF_4$:Ln^{3+} core nanospheres via a two-step thermal decomposition process [45]. The resultant $NaYF_4$@$NaGdF_4$ core−shell nanoparticles exhibited different up-/down-conversion luminescence under irradiation of a 980 nm laser and a 254 nm UV light, respectively. However, most of these dual-mode $NaREF_4$:Ln^{3+} luminescent materials with core−shell structure are synthesized through thermal decomposition method using organometallic compounds as precursors, which provides hydrophobic nature and poor surface conjugation activity of the materials. More importantly, the $NaREF_4$:Ln^{3+} luminescent materials synthesized by thermal decomposition method often have low fluorescence quantum yield (low luminescent intensity) owing to the surface defect generated during the thermal decomposition process [47−49].

To develop a facile and versatile strategy for the synthesis of hydrophilic dual-mode fluorescent materials with high luminescent intensity, the preparation of monodisperse hydrophilic $NaYF_4$:Yb^{3+},Tm^{3+}@$NaGdF_4$:Ce^{3+},Eu^{3+} double-jacket microtubes (DJMTs) by coating $NaGdF_4$:Ce^{3+},Eu^{3+} shell onto $NaYF_4$:Yb^{3+},Tm^{3+} parent microtubes via a PAA-mediated hydrothermal process was reported. The morphology, structure, composition of the DJMTs were carefully characterized. Besides, the growing mechanism of the $NaGdF_4$:Ce^{3+},Eu^{3+} shell on the surface of the $NaYF_4$:Yb^{3+},Tm^{3+} parent microtube was systematically investigated. The resultant hydrophilic DJMTs were subsequently made into environmentally benign luminescent inks. Eventually, the concealed and dual-mode luminescent anti-counterfeiting patterns were successfully printed on the paper based on the as-prepared DJMT inks via inkjet printing technology.

2 Experimental

2.1 Chemicals and materials

$YCl_3\cdot 6H_2O$ (99.9%), $YbCl_3\cdot 6H_2O$ (99.9%), $TmCl_3\cdot 6H_2O$ (99.9%), $GdCl_3\cdot 6H_2O$ (99.9%), $CeCl_3\cdot 6H_2O$ (99.9%), $EuCl_3\cdot 6H_2O$ (99.9%), sodium fluoride (NaF), and glycerin were purchased from Shanghai Aladdin Chemistry Co., Ltd. (China). Poly(acrylic acid) (PAA) (average relative molecular mass 240000 g/mol, and 25 wt.% solution in water) was obtained from Acros. All other chemicals were of analytical reagent grade and used without further purification. All solutions used in this work were prepared with deionized water. The printing substrate of duplicating paper without fluorescence was purchased from Double A (1991) Public Co., Ltd.

2.2 Synthesis of $NaYF_4$:Yb^{3+},Tm^{3+} parent upconversion microparticles (UCMPs)

The $NaYF_4$:Yb^{3+},Tm^{3+} core UCMPs were synthesized via a poly(acrylic acid) (PAA) assisted hydrothermal process as discussed in our previous work [50]. Typically, 236.6 mg (0.78 mmol) $YCl_3\cdot 6H_2O$, 77.5 mg (0.20 mmol) $YbCl_3\cdot 6H_2O$, and 7.6 mg (0.020 mmol) $TmCl_3\cdot 6H_2O$ were dissolved in 5 mL H_2O with magnetic stirring to form the rare earth chloride aqueous solution. Then, a mixture of 15 mL ethanol and 6 mL PAA (10 wt.%) aqueous solution containing PAA (2.8×10^{-6} mol) was added into the rare earth chloride aqueous solution. After being stirred for 30 min, 8 mL (1.0 mol/L) of NaF (8.0 mmol) aqueous solution was slowly added into the above reaction system under vigorous stirring to form a well-dispersed milky solution. The pH value of the mixture was adjusted at 5.0 by hydrochloric acid (2.0 mol/L). The reaction mixture was stirred at room temperature for 1 h and then transferred into a Teflon bottle held in a stainless steel autoclave, sealed, and maintained at 200 °C for 24 h. After the completion of the hydrothermal reaction, the autoclave was cooled to room temperature naturally. The resulting precipitates were separated by centrifugation at 3000 r/min for 10 min, washed with ethanol/deionized water (volume ratio of 1:1) three times, and finally dried at 60 °C for 12 h to obtain the $NaYF_4$:Yb^{3+},Tm^{3+} UCMPs as a white powder.

2.3 Synthesis of $NaYF_4$:Yb^{3+},Tm^{3+}@$NaGdF_4$:Ce^{3+},Eu^{3+} DJMTs

$NaYF_4$:Yb^{3+},Tm^{3+}@$NaGdF_4$:Ce^{3+},Eu^{3+} DJMTs were obtained by epitaxial growth of $NaGdF_4$:Ce^{3+},Eu^{3+} shell onto the $NaYF_4$:Yb^{3+},Tm^{3+} UCMPs using hydrothermal reaction. Typically, 31.6 mg (0.085 mmol) $GdCl_3\cdot 6H_2O$, 3.7 mg (0.010 mmol) $CeCl_3\cdot 6H_2O$ and 1.8 mg (0.005 mmol) $EuCl_3\cdot 6H_2O$ were dissolved in 5 mL H_2O with magnetic stirring. Then, a mixture of 15 mL ethanol and 6 mL PAA (10 wt.%) aqueous solution containing PAA (2.8×10^{-6} mol) was added into the above solution. After stirring for 30 min, 8 mL (1.0 mol/L) of NaF (8.0 mmol) aqueous solution was slowly added into the reaction system under vigorous stirring. The pH value of the mixture was adjusted at 5.0 by hydrochloric acid (2.0 mol/L). Then, 8 mL aqueous solution containing 0.1 g UCMPs was added in the reaction system and further stirred at room temperature for 1 h. Finally, the mixture solution was transferred into a Teflon bottle held in a stainless steel autoclave, sealed, and maintained at 200 °C for 24 h. After the completion of the hydrothermal reaction, the autoclave was cooled to room temperature naturally. The resulting precipitates were separated by centrifugation at 3000 r/min for 10 min, washed with ethanol/deionized water (volume ratio of 1:1) three times, and finally dried at 60 °C for 12 h to obtain the $NaYF_4$:Yb^{3+},Tm^{3+}@$NaGdF_4$:Ce^{3+},Eu^{3+} DJMTs as a white powder.

2.4 Formulation of hydrophilic dual-mode luminescent DJMTs inks

The hydrophilic dual-mode luminescent DJMT inks were fabricated by dispersing the as-synthesized DJMTs in a mixture solvent of ethanol, deionized water, and glycerol. In order to obtain luminescent inks with the optimal performance such as viscosity and surface tension, the mass ratio of ethanol, water, to glycerol was kept at 40:40:20. Typically, 0.1 g DJMTs were added to 10.0 g mixture solvent (4.0 g ethanol, 4.0 g deionized water, and 2.0 g glycerol). Then, the resulting mixture was vigorously stirred for 20 min and followed by 10 min sonication to achieve the well dispersion of DJMTs.

2.5 Characterization and instrument

The phase purity and crystallinity of the as-prepared particles were characterized by X-ray diffraction (XRD) using a Rigaku Model D/max−2500 diffractometer, with Cu K_α radiation in the 2θ range of 10°−80° with a step size of 0.02°. Fourier transform infrared spectroscopy (FTIR) was recorded on a Nicolet 380 spectrometer using 32 scans and a 4 cm^{-1} resolution. Field emission scanning electron microscopy (FE-SEM) images were obtained with Hitachi S−3000N instrument. Transmission electron microscopy (TEM) was obtained from a JEM−1011 instrument operating at an accelerating voltage of 100 kV. X-ray photoelectron spectroscopy (XPS) spectra were obtained with a PHI 5000 Versa Probe system, using a monochromatic Al K_α X-ray source. The emission spectra of the products were carried out using a Hitachi F−4500 5J2−0004 spectrophotometer with an external CNI (5W) 980 nm IR fiber coupled laser system (Changchun New Industries Optoelectronics Tech. Co., Ltd.). The inkjet printing of the DJMT inks was performed on a Canon PIXMA ip2780 inkjet printer equipped with 25 pL cartridge (PG-815) and 2.5 pL cartridge (PG-816). The PG-815 cartridge was capable of generating ink droplets as small as about 36 μm in diameter. The photographs of the sample under the 980 nm laser irradiation (5 W) were obtained using a Nikon D7000 camera with an infrared filter. The exposure time was 15 s, aperture size used was F14 and photosensibility (ISO) was 3200.

3 Results and discussion

Scheme 1 briefly describes a general procedure for the synthesis and inkjet printing of $NaYF_4$:Yb^{3+},Tm^{3+}@$NaGdF_4$:Ce^{3+},Eu^{3+} DJMTs for the application of dual-mode fluorescent anti-counterfeiting. To this end, $NaYF_4$:Yb^{3+},Tm^{3+} upconversion microtubes were firstly synthesized via a PAA mediated hydrothermal process. Subsequently, a $NaGdF_4$:Ce^{3+},Eu^{3+} shell with down-conversion luminescence was epitaxially grown onto the surface of $NaYF_4$:Yb^{3+},Tm^{3+} UCMPs via a

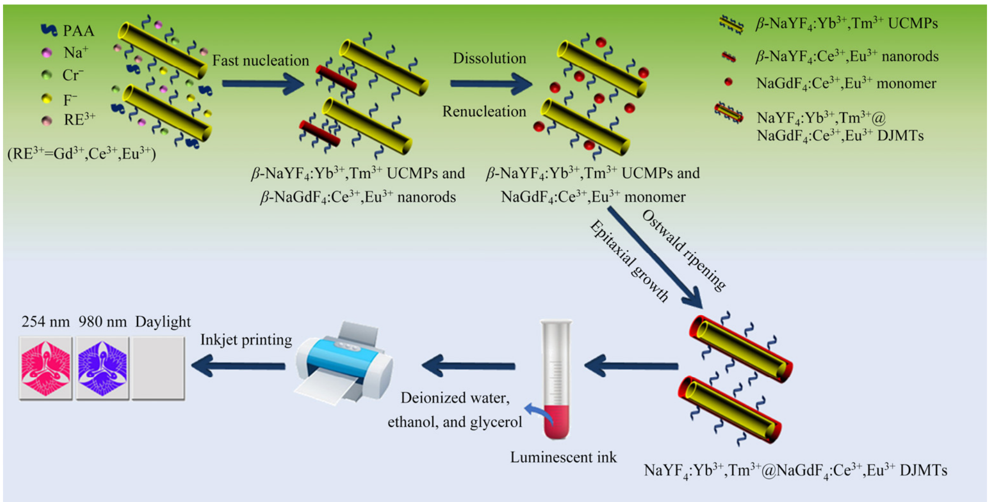

Scheme 1 Schematic diagram of synthesis and inkjet printing of dual-mode $NaYF_4$:Yb^{3+},Tm^{3+}@$NaGdF_4$:Ce^{3+},Eu^{3+} DJMTs for anti-counterfeiting application

secondary PAA mediated hydrothermal process. The resultant NaYF$_4$:Yb^{3+},Tm^{3+}@NaGdF$_4$:Ce^{3+},Eu^{3+}generally presented as a double-jacket microtube structure with upconversion/downconversion dual-mode luminescence and hydrophilic surface. Then, the as-obtained NaYF$_4$:Yb^{3+},Tm^{3+}@NaGdF$_4$:Ce^{3+},Eu^{3+} DJMTs were dispersed into a mixture solvent of ethanol, deionized water, and glycerol to produce environmentally benign dual-mode luminescent DJMT inks. Finally, the dual-mode luminescent DJMT inks were inkjet-printed on paper substrates for creation of pre-designed dual-mode luminescent anti-counterfeiting patterns.

3.1 Characterization of NaYF$_4$:Yb^{3+},Tm^{3+}@NaGdF$_4$:Ce^{3+},Eu^{3+} DJMTs

Field emission scanning electron microscope (FE-SEM), X-ray diffraction (XRD), and transmission electron microscopy (TEM) were adopted to characterize the morphology and structure of the as-synthesized NaYF$_4$:Yb^{3+},Tm^{3+}@NaGdF$_4$:Ce^{3+},Eu^{3+} DJMTs. As shown in Fig. 1, the XRD pattern of NaYF$_4$:Yb^{3+},Tm^{3+} UCMPs showed typical standard pattern of hexagonal-phase NaYF$_4$ (JCPDS: 28-1192), and no other phases were observed, indicating Yb^{3+} and Tm^{3+} ions were successfully doped into the β-NaYF$_4$ lattice [35]. Compared with the XRD pattern of NaYF$_4$:Yb^{3+},Tm^{3+} UCMPs, an additional weak diffraction peak at 2θ=42.71° (as indicated by the black arrow) emerged after the epitaxial growth of NaGdF$_4$:Ce^{3+},Eu^{3+} shell, which can be indexed as (201) planes of β-NaGdF$_4$ (JCPDS No. 27-0699) [51]. Besides, the peak at 2θ=29.92° became broader than that on XRD pattern of NaYF$_4$:Yb^{3+},Tm^{3+} UCMPs core, which might be due to the merging of the diffraction peak at 2θ=29.65° indexed as the (110) planes of β-NaGdF$_4$ (JCPDS No. 27-0699) and the diffraction peak at 2θ=29.96° indexed as the (110) planes of β-NaYF$_4$ (JCPDS No. 28-1192). The results collectively suggested the formation of hexagonal-phase NaYF$_4$:Yb^{3+},Tm^{3+}@NaGdF$_4$:Ce^{3+},Eu^{3+} composites.

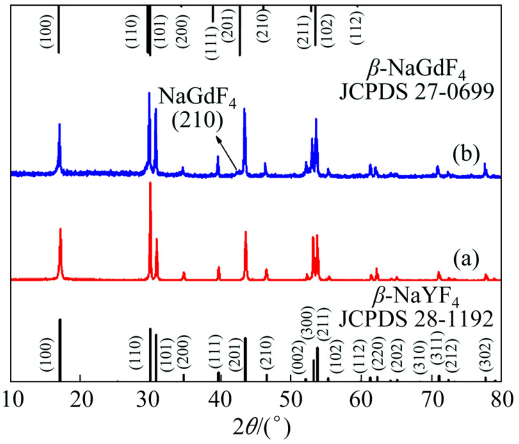

Fig. 1 XRD patterns of UCMPs (a) and DJMTs (b) in comparison with standard data of β-NaYF$_4$ (JCPDS No. 28-1192) and β-NaGdF$_4$ (JCPDS No. 27-0699)

Figures 2(a, b) exhibit the representative FE-SEM images of NaYF$_4$:Yb^{3+},Tm^{3+} UCMPs and NaYF$_4$:Yb^{3+},Tm^{3+}@NaGdF$_4$:Ce^{3+},Eu^{3+} DJMTs. It can be seen that the NaYF$_4$:Yb^{3+},Tm^{3+} UCMPs were monodisperse hexagonal microtubes with length and diameter of around 2.0 and 0.6 μm, respectively (Fig. 2(a)). After implementing the epitaxial growth, the resultant NaYF$_4$:Yb^{3+},Tm^{3+}@NaGdF$_4$:Ce^{3+},Eu^{3+} DJMTs still retained the uniform hexagonal microtube morphology (no additional crystals were found), as shown in Fig. 2(b). The results potentially suggested the NaGdF$_4$:Ce^{3+},Eu^{3+} crystals were formed and coated on the surface of NaYF$_4$:Yb^{3+},Tm^{3+} UCMPs. SEM elemental mapping of a single DJMTs in Fig. 3 gave more evidences about the formation of NaYF$_4$:Yb^{3+},Tm^{3+}@NaGdF$_4$:Ce^{3+},Eu^{3+} composite since all the lanthanide elements (Y, Yb, Tm, Gd, Ce and Eu) were located in a single NaYF$_4$:Yb^{3+},Tm^{3+}@NaGdF$_4$:Ce^{3+},Eu^{3+} DJMT. It should be noted that the coating amount of NaGdF$_4$:Ce^{3+},Eu^{3+} shell was very low, which can not lead to a significant size change detected by SEM observation. To further demonstrate the double-jacket microtube structure and make an observation of the size change, TEM elemental mapping was performed. Figure 2(c) shows TEM image of typical NaYF$_4$: Yb^{3+},Tm^{3+}@NaGdF$_4$:Ce^{3+},Eu^{3+} DJMTs, which represented a microtube with the length and diameter of ~2.0 μm and ~0.6 μm, respectively. From the TEM elemental mapping (Figs. 2(d−f)), it can be clearly seen that the Gd^{3+} ions (cyan) originated from NaGdF$_4$:Ce^{3+},Eu^{3+} were uniformly distributed at the outer shell of the microtube (Fig. 2(e)) and Y^{3+} ions (red) originated from the parent NaYF$_4$:Yb^{3+},Tm^{3+} microtube were located at the inner pot of the double-jacket microtube (Fig. 2(d)), demonstrating the core−shell structure of the NaYF$_4$:Yb^{3+},Tm^{3+}@NaGdF$_4$:Ce^{3+},Eu^{3+} DJMTs. Based on the elemental mapping image of Y^{3+} and Gd^{3+} ions (Fig. 2(f)), it

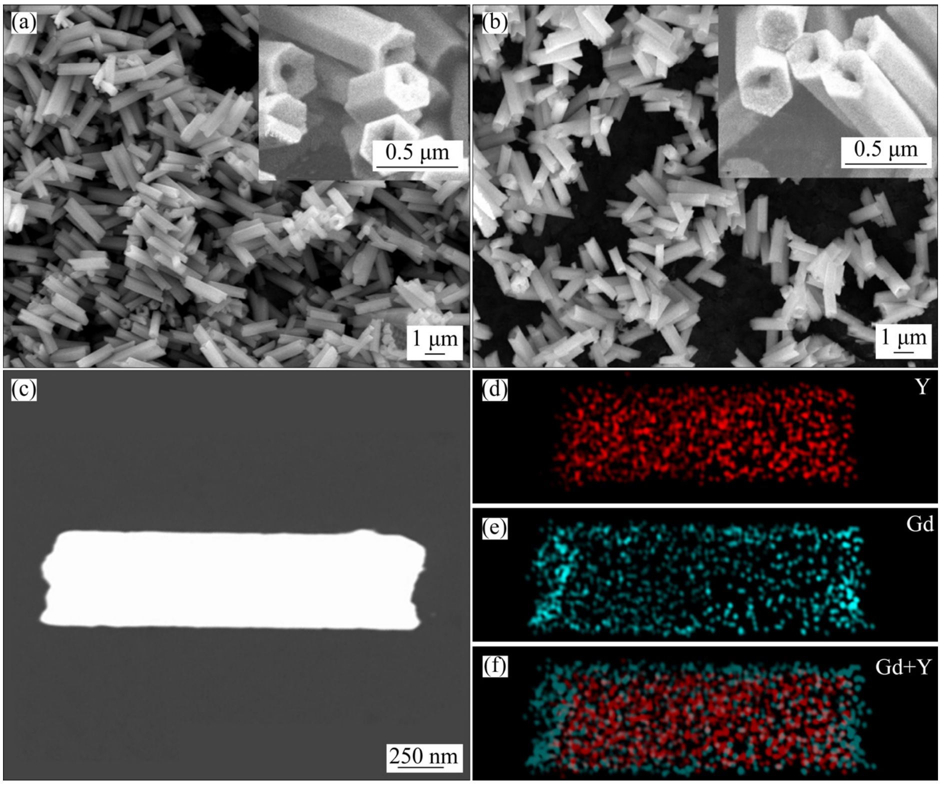

Fig. 2 Typical FE-SEM, TEM and elemental mappings of as-prepared microparticles: (a) UCMPs; (b) DJMTs; (c) TEM image; (d−f) Elemental mappings

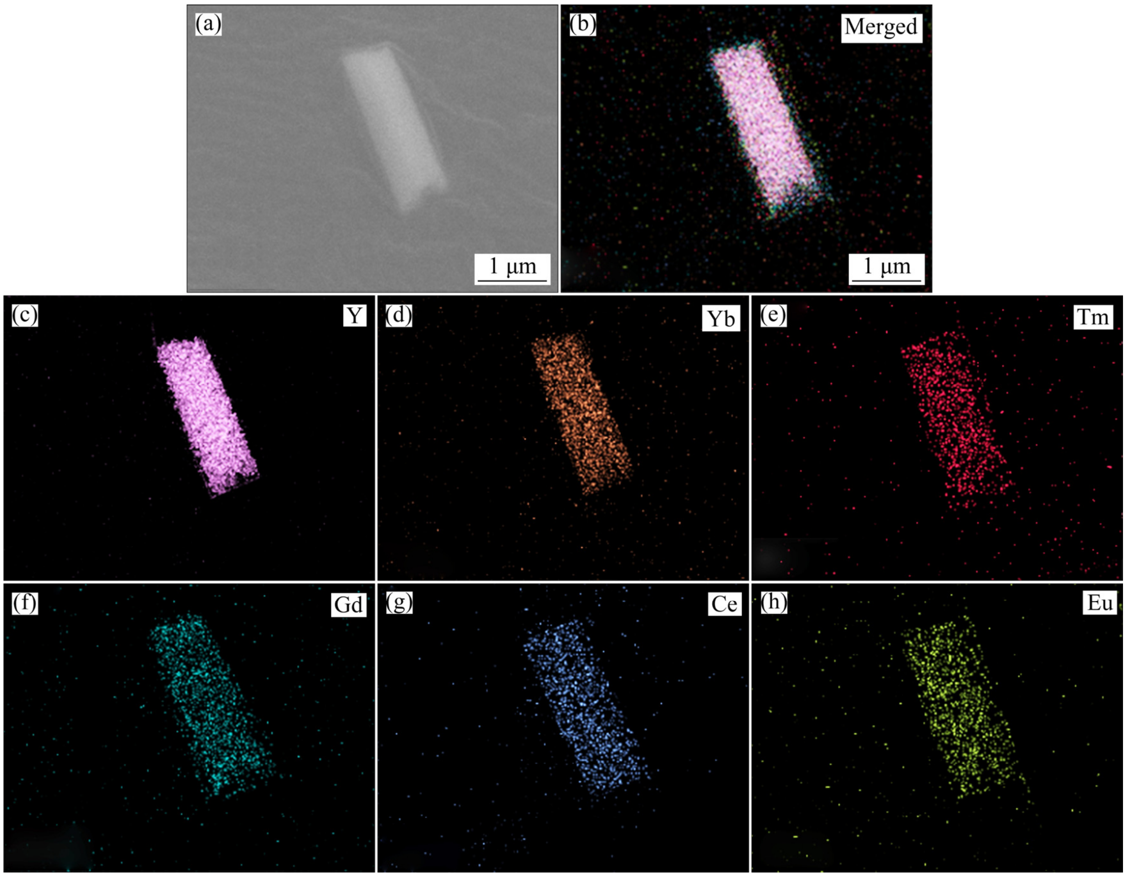

Fig. 3 SEM image of DJMTs (a), merged element map (b) and different element maps of Y (c), Yb (d), Tm (e), Gd (f), Ce (g) and Eu (h) elements

can be estimated that the coating of $NaGdF_4$:Ce^{3+},Eu^{3+} onto the surface of $NaYF_4$:Yb^{3+},Tm^{3+} UCMPs resulted in the size of $NaYF_4$:Yb^{3+},Tm^{3+}@$NaGdF_4$:Ce^{3+},Eu^{3+} DJMTs with 100 nm increased in length and 40 nm increased in diameter.

Figure 4(a) shows the full XPS spectra of the $NaYF_4$:Yb^{3+},Tm^{3+} UCMPs and $NaYF_4$:Yb^{3+},Tm^{3+}@$NaGdF_4$:Ce^{3+},Eu^{3+} DJMTs. As shown, electron binding energy peaks at 1072.0, 685.0, 160.0 and 302.0 eV corresponding to the Na 1s, F 1s, Y 3d, and Y 3p in the $NaYF_4$:Yb^{3+},Tm^{3+} were detected in the full XPS spectrum of $NaYF_4$:Yb^{3+},Tm^{3+} UCMPs. Besides, electron binding energy peaks at 285.0 and 532.0 eV corresponding to the C 1s and O 1s originated from PAA molecules on the surface of $NaYF_4$:Yb^{3+},Tm^{3+} UCMPs were also observed, potentially suggesting that the surface of $NaYF_4$:Yb^{3+},Tm^{3+} UCMPs was decorated by PAA molecule. Similarly, the elements including Na 1s, F 1s, C 1s and O 1s were also detected in the full

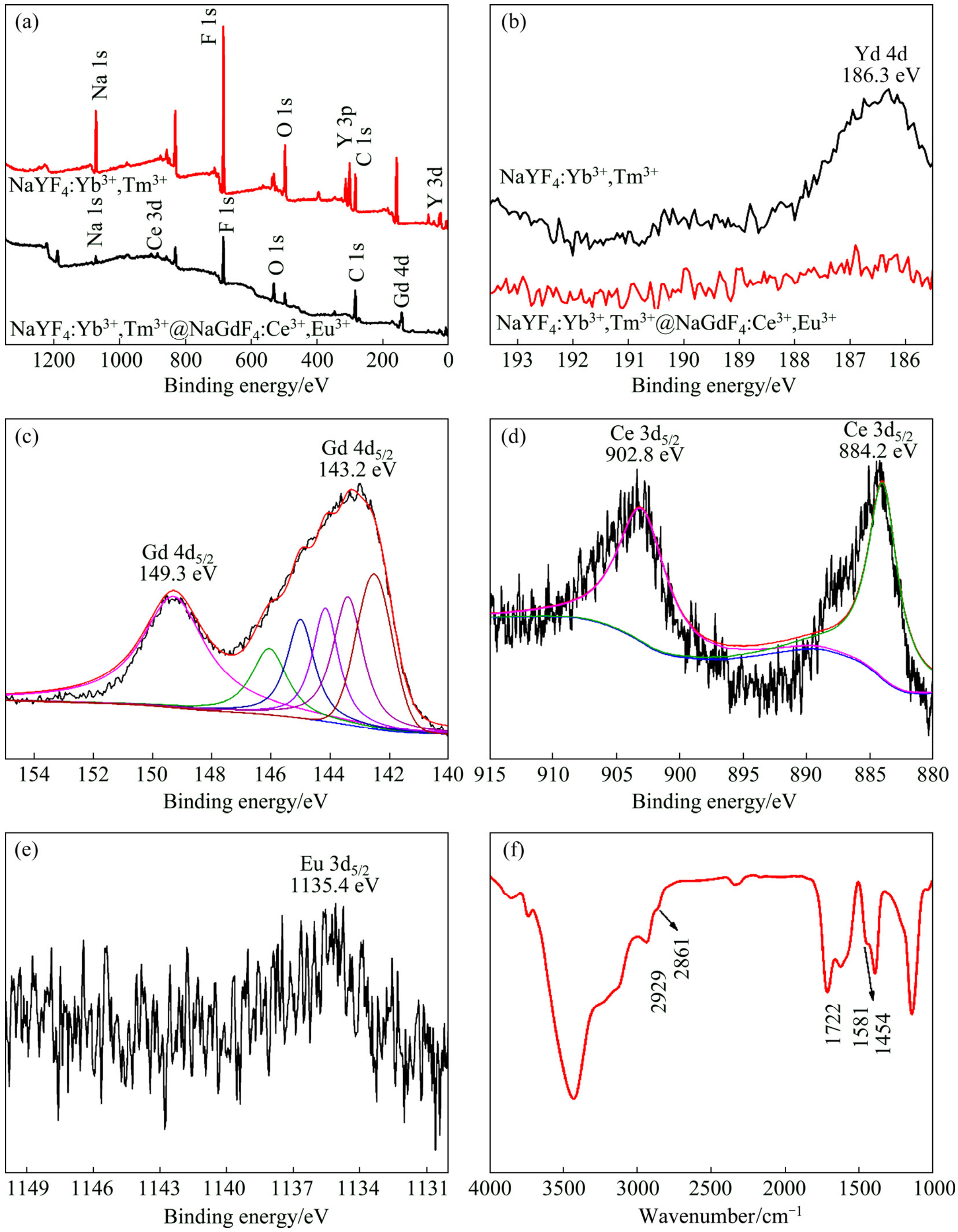

Fig. 4 XPS spectra of as-prepared UCMPs and DJMTs: (a) Survey spectrum; (b−e) High-resolution spectra of Yb 4d, Gd 4d, Ce 3d and Eu $3d_{5/2}$; (f) FT-IR spectra of DJMTs

XPS spectrum of $NaYF_4$:Yb^{3+},Tm^{3+}@$NaGdF_4$:Ce^{3+},Eu^{3+} DJMTs. Differently, instead of Y 3d and Yb 3d, electron binding energy peaks at 143.2 and 884.2 eV corresponding to the Gd 4d and Ce 3d in $NaGdF_4$:Ce^{3+},Eu^{3+} were detected. The disappearance of the Yb 3d peak was demonstrated by the comparison of the two XPS spectra in the range of 193−186 eV, as shown in Fig. 4(b). Furthermore, the characteristic peaks at 149.3 and 143.2 eV for Gd 4d, 902.8 and 884.2 eV for Ce 3d, and 1135.4 eV for Eu $3d_{5/2}$ were also observed in the magnified XPS spectra range of 155−140 eV (Fig. 4(c)), 915−880 eV (Fig. 4(d)), and 1150−1130 eV (Fig. 4(e)), respectively. These surface elemental changes demonstrated the core−shell structure of the $NaYF_4$:Yb^{3+},Tm^{3+}@$NaGdF_4$:Ce^{3+},Eu^{3+} DJMTs, where $NaGdF_4$:Ce^{3+},Eu^{3+} was coated on the surface of the $NaYF_4$:Yb^{3+},Tm^{3+} microtube. The surface chemical component of $NaYF_4$: Yb^{3+},Tm^{3+}@$NaGdF_4$:Ce^{3+},Eu^{3+} DJMTs was further characterized by FT-IR. As shown in Fig. 4(f), the characteristic peaks of PAA molecules at 2929 and 2861 cm^{-1} were assigned to the asymmetric and symmetric stretching vibrations of the methylene (—CH_2) in the long alkyl chain. 1581 and 1454 cm^{-1} associated with the asymmetric and symmetric stretching vibrations of carboxylate anions, and 1722 cm^{-1} corresponding to the vibration of carbonyl group were clearly seen, indicating that the surface of $NaYF_4$:Yb^{3+},Tm^{3+}@$NaGdF_4$:Ce^{3+},Eu^{3+} DJMTs was decorated by PAA molecule, rendering its hydrophilic nature [52].

The dual-mode luminescent property of the $NaYF_4$:Yb^{3+},Tm^{3+}@$NaGdF_4$:Ce^{3+},Eu^{3+} DJMTs was studied by upconversion and downconversion fluorescence spectrum. It is generally accepted that constructing a core−shell structure can decrease the non-radiative decay of the upconversion materials caused by surface defects and vibrational deactivation from solvent molecules, which will improve the UC fluorescence intensity of the upconversion materials under NIR irradiation [53]. In this study, we compared the UC fluorescence properties of UCMPs with a sole core structure and DJMTs with a core−shell structure in aqueous solution under 980 nm laser. As shown in Fig. 5(a), both UCMPs and DJMTs exhibited typical UC fluorescent emission peaks of $NaYF_4$:Yb^{3+},Tm^{3+}

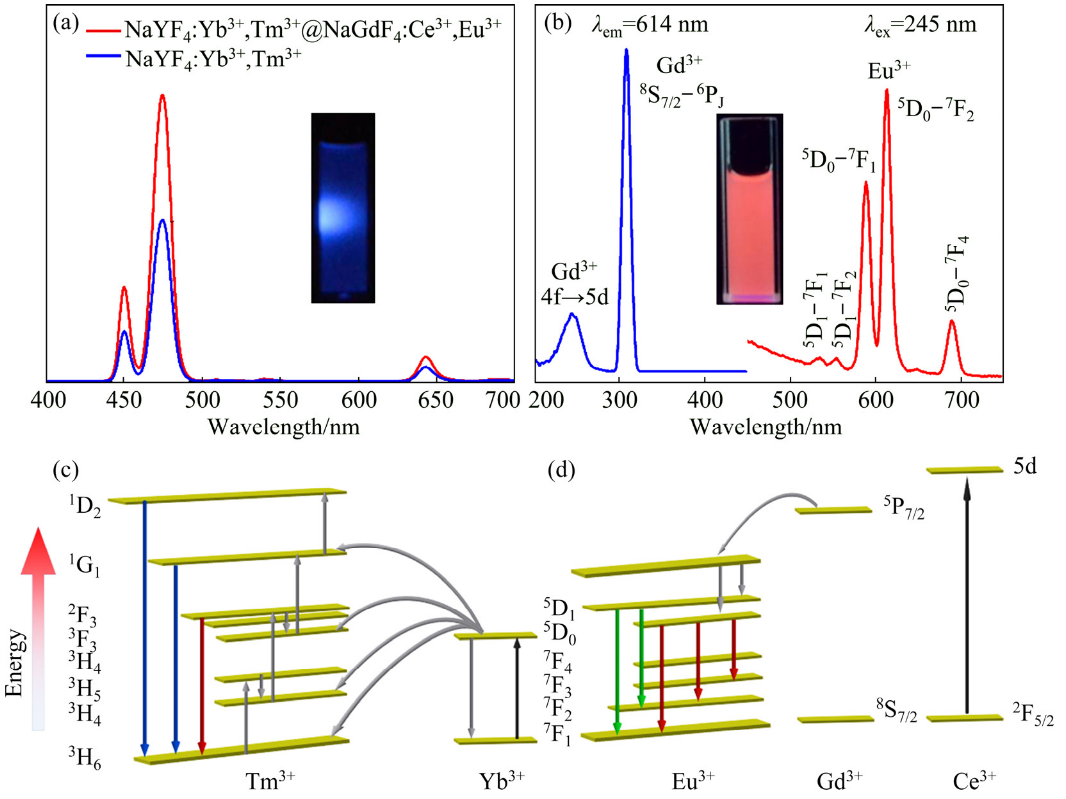

Fig. 5 Comparison of UC luminescent properties of UCMPs and DJMTs (a), excitation and emission spectra of DJMTs with excitation spectrum monitored at 614 nm and emission spectrum at 254 nm (b), UC energy transfer of processes of Yb^{3+}−Tm^{3+} in both UCMPs and DJMTs (c), and ultraviolet excitation energy absorbed by Ce^{3+} sensitizer and transferred to Gd^{3+}, followed by energy transfer to lanthanide emitter Eu^{3+} in DJMTs (d)

located at the same positions of 450, 475 and 644 nm. These three peaks were assigned to the $^1D_2$–$^3F_4$, $^1G_4$–$^3H_6$, and $^1G_4$–$^3F_4$ transitions of Tm^{3+}, respectively (Fig. 5(c)). Since the intensity of blue emission peaks was significantly higher than that of the red peak, both UCMPs and DJMTs would exhibit a dominant blue color under the 980 nm laser irradiation (as shown in the inset of Fig. 5(a)). Besides, the DJMTs emitted 1.76 times higher UC luminescence than UCMPs, confirming that the core−shell structure resulted in an enhanced UC luminescence. Figure 5(b) shows the excitation and emission spectra of the $NaYF_4$:Yb^{3+},Tm^{3+}@$NaGdF_4$:Ce^{3+},Eu^{3+} DJMTs in aqueous solutions under the irradiation of 641 and 254 nm laser, respectively. As can be seen, the excitation spectra of DJMTs consisted of a broad band at 254 nm and a sharp line at 310 nm, which were ascribed to the $^2F_{5/2}$–5d transition of Ce^{3+} and the $^8S_{7/2}$–$^6P_{7/2}$ transition of Gd^{3+}, respectively, implying there was an efficient energy transfer from Ce^{3+} and Gd^{3+} to the Eu^{3+} [54]. On the emission spectrum under the irradiation of 254 nm laser, five emission peaks of Eu^{3+} as activator ion at 534, 554, 591, 614 and 691 nm were detected, corresponding to the transitions of $^5D_1$–$^7F_1$, $^5D_1$–$^7F_2$, $^5D_0$–$^7F_1$, $^5D_0$–$^7F_2$ and $^5D_0$–$^7F_4$ of Eu^{3+}, respectively (Fig. 5(d)). Clearly, the intensity of red emission peaks at 591 and 614 nm was significantly higher than that of other peaks. Therefore, the DJMTs showed a dominant red color under the irradiation of 254 nm laser (as shown in the inset of Fig. 5(b)).

3.2 Growing mechanism

In the synthesis, PAA played an important role in guiding the direct growth of $NaGdF_4$:Ce^{3+},Eu^{3+} shell onto the surface of $NaYF_4$:Yb^{3+},Tm^{3+} parent microtubes. A comparative experiment was conducted by similar hydrothermal process without the adding of PAA. The SEM image of the resultant crystals is shown in Fig. 6. As shown, the resultant crystals showed a mixture of microtubes and some irregular microparticles, as indicated by the stained part in Fig. 6. Nevertheless, uniform microtubes were obtained in PAA mediated hydrothermal growth of $NaGdF_4$:Ce^{3+},Eu^{3+} shell (Fig. 2(b)). The results suggested that the PAA played a critical role in determining the particle growth and shape evolution.

To understand the growing mechanism of $NaYF_4$:Yb^{3+},Tm^{3+}@$NaGdF_4$:Ce^{3+},Eu^{3+} DJMTs, the hydrothermal reaction in different time intervals of 0, 3, 6, 9 and 12 h was conducted. The intermediate products were subjected to XRD and FE-SEM characterization. Figure 7 shows the XRD patterns of samples prepared at different reaction time intervals. As shown in Fig. 7(a), before the reaction, the $NaYF_4$:Yb^{3+},Tm^{3+} UCMPs were pure hexagonal phase $NaYF_4$. Upon the hydrothermal treatment for 3 h, a hexagonal phase $NaGdF_4$ (β-$NaGdF_4$) emerged in the presence of hexagonal phase $NaYF_4$ as evidenced by the small (110) peak at 2θ=29.92° and the (201) peak at 2θ=42.71° (Fig. 7(b)), suggesting that the sample was a mixture of hexagonal phase $NaYF_4$ and $NaGdF_4$. With the reaction prolonging, the peaks at 2θ=29.92° and 42.71° were weakened (as shown in Figs. 7(c, d)), potentially suggesting that prolonged hydrothermal treatment led to the dissolution of β-$NaGdF_4$. After

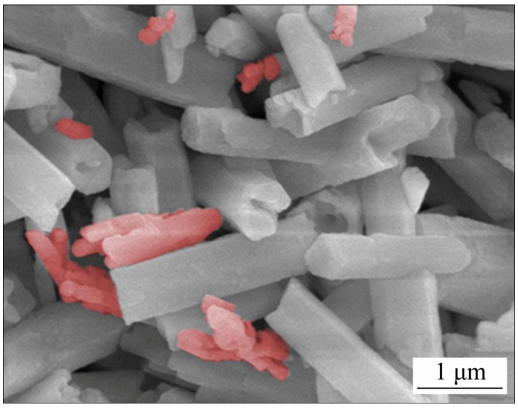

Fig. 6 FE-SEM image of DJMTs prepared without addition of PAA

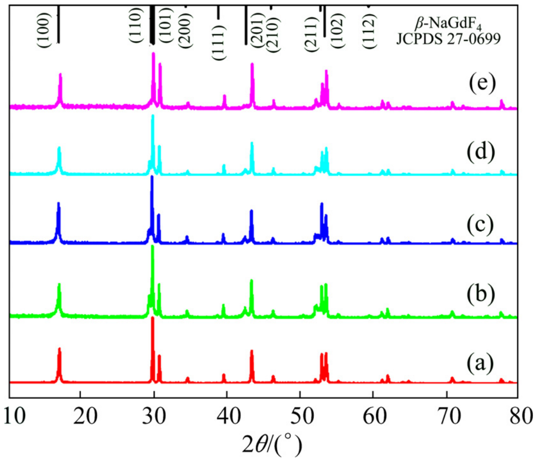

Fig. 7 XRD patterns of intermediates obtained at different reaction time intervals: (a) 0 h; (b) 3 h; (c) 6 h; (d) 9 h; (e) 12 h

12 h of hydrothermal treatment, the (110) peak of β-$NaGdF_4$ at 2θ=29.92° can not be clearly seen, but the (110) peak of β-$NaYF_4$ at 2θ=29.92° was broadened, which may be due to the merging of the (110) peak of β-$NaGdF_4$ at 2θ=29.92° and the (110) peak of β-$NaYF_4$ at 2θ=29.92°. Besides, the (201) peak of β-$NaGdF_4$ at 2θ=42.71° turned to be a broad halo peak, as shown in Fig. 7(e). This phenomenon implied the formation of β-$NaYF_4$@β-$NaGdF_4$ composite materials. Based on the XRD results, we deduced that the growth of $NaGdF_4:Ce^{3+},Eu^{3+}$ shell experienced a process of generation of β-$NaGdF_4$ and β-$NaYF_4$ mixture firstly, and the formation of β-$NaYF_4$@β-$NaGdF_4$ composite materials ultimately.

Further, the morphology of the intermediate products was checked to make a clear observation on the growth of the $NaGdF_4:Ce^{3+},Eu^{3+}$ shell. The FE-SEM images of the intermediate products are shown in Fig. 8. Initially, UCMPs presented as uniform hollow microtubes, as described in Fig. 2(a). Upon 3 h of hydrothermal reaction, the resultant crystals contained not only the UCMPs but also many small microrods (~700 nm in length and ~200 nm in diameter) (Fig. 8(a)). The small microrods might be due to the fast nucleation of Ln^{3+} (Gd^{3+}, Ce^{3+}, Eu^{3+}) with sodium and fluoride ion and the formation of $NaGdF_4:Ce^{3+},Eu^{3+}$ crystals. The results were in good agreement with the XRD results where the hexagonal phase of $NaGdF_4$ (β-$NaGdF_4$) emerged. As the reaction proceeded, the small microrods gradually disappeared, as shown in Figs. 8(b, c). The gradual disappearance of the microrods suggested that there existed a dissolution-renucleation of β-$NaGdF_4:Ce^{3+},Eu^{3+}$. This meant that the β-$NaGdF_4:Ce^{3+},Eu^{3+}$ microrods gradually dissolved as crystal monomer with the proceeding of the reaction. In one aspect, the monomer tended to deposit on the surface of the UCMPs to decrease their surface energy, known as the Ostwald ripening phenomenon. In the other aspect, the PAA polymer on the prismatic planes ({1010} crystal planes) was more than that on the top/bottom facets ({0001} crystal planes) due to the large surface area, and the negatively charged PAA polymer would adsorb the monomer, which promoted the growth of the β-$NaGdF_4:Ce^{3+},Eu^{3+}$ shell and the formation of DJMTs. The products can be indexed as uniform DJMTs after 12 h of hydrothermal reaction, as shown in Fig. 8(d). The growing process is schematically shown in Scheme 1.

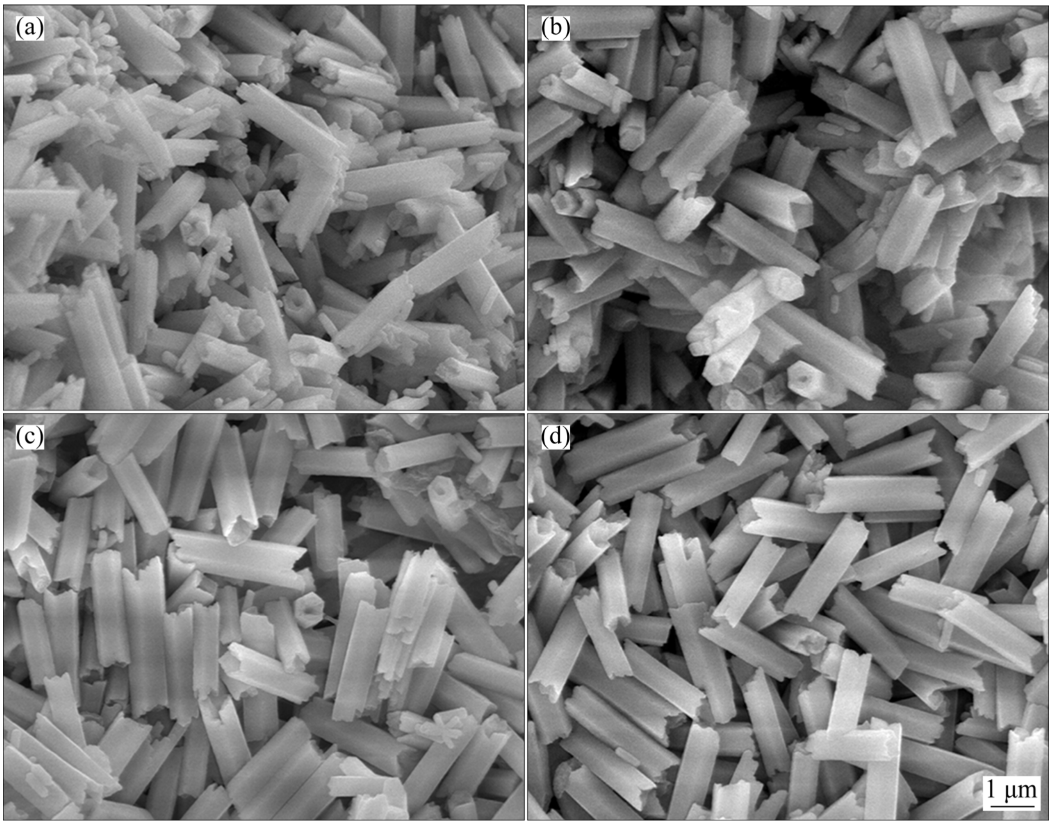

Fig. 8 FE-SEM images of intermediates obtained at different reaction time intervals: (a) 3 h; (b) 6 h; (c) 9 h; (d) 12 h

3.3 Inkjet printing and anti-counterfeiting application

Taking advantages of the dual-mode responsive fluorescence and good water-dispersion ability, the DJMTs are believed to be a promising luminescent material for anti-counterfeiting applications. As a proof-of-concept, dual-mode luminescent inks were prepared by dispersing DJMTs into a mixed solvent of ethanol, water, and glycerol (40:40:20, mass ratio). We used the dual-mode responsive fluorescence DJMTs ink to construct fluorescence patterns by inkjet printing technology. Initially, we printed a complicated pattern on normal printing paper. As shown in Fig. 9(a), no printing imprints and visible pattern were observed under daylight. However, a red pattern and a blue pattern can be read out under the irradiation of a 254 nm UV lamp and a 980 nm laser, respectively. To develop more advanced anti-counterfeiting technique, we intended to design a complex quick-response (QR) code using the dual-mode fluorescent DJMT ink and single-mode fluorescent UCMP ink. The design principle is schematically shown in Fig. 9(b). We divided a QR code into two sections. One contained three squares at the three corners of the QR code, and the left fragmentary QR code was set as the other section. The three squares were inkjet-printed on the paper substrate using the dual-mode fluorescent DJMT ink and the left fragmentary QR code was inkjet-printed by using the single-mode fluorescent UCMP ink at proper location, as shown in Fig. 9(b). The printing process can be controlled on a computer. Similarly, no visible pattern was observed under daylight, but three red squares can be read out under a 254 nm UV lamp and an integral QR code can be read out under a 980 nm laser, as shown in Fig. 9(c). We believed that this anti-counterfeiting technique was more complicated and would have great potential in high level of anti-counterfeiting applications.

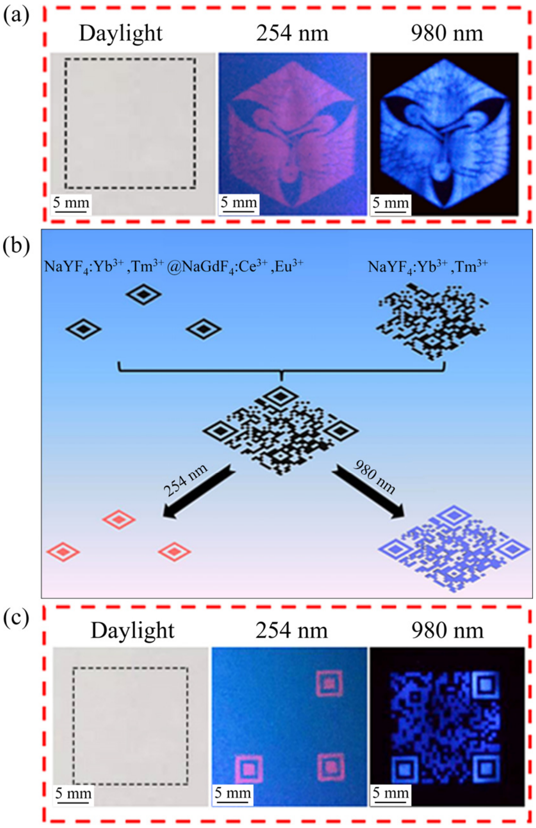

Fig. 9 Photographs of formulated dual-mode responsive fluorescence DJMT ink and printed patterns under irradiation of 254 and 980 nm (a), and possible luminescence anti-counterfeiting application using UCMP and DJMT ink (b, c)

4 Conclusions

(1) Mono-dispersed hydrophilic NaYF$_4$:Yb^{3+},Tm^{3+}@NaGdF$_4$:Ce^{3+},Eu^{3+} double-jacket microtubes (DJMTs) with upconversion/downconversion dual-mode luminescence were successfully prepared by coating NaGdF$_4$:Ce^{3+},Eu^{3+} shell on the surface of NaYF$_4$:Yb^{3+},Tm^{3+} hollow microtube via hydrothermal method using PAA as structure directing agent and ligand.

(2) The growth of NaGdF$_4$:Ce^{3+},Eu^{3+} shell experienced a crystal phase transition from β-NaGdF$_4$ and β-NaYF$_4$ mixture to β-NaYF$_4$@β-NaGdF$_4$ composite crystal, and morphology evolution from mixture of β-NaGdF$_4$:Ce^{3+},Eu^{3+} nanorods and β-NaYF$_4$:Yb^{3+},Tm^{3+} microtubes to NaYF$_4$:Yb^{3+},Tm^{3+}@NaGdF$_4$:Ce^{3+},Eu^{3+} DJMTs. The formation mechanism of DJMTs was the dissolution−renucleation of β-NaGdF$_4$:Ce^{3+},Eu^{3+} microrods and the growth of β-NaGdF$_4$:Ce^{3+},Eu^{3+} shell via the classical Ostwald ripening mechanism under the hydrothermal condition.

(3) The as-prepared NaYF$_4$:Yb^{3+},Tm^{3+}@NaGdF$_4$:Ce^{3+},Eu^{3+} DJMTs can be made into luminescent ink and can be inkjet-printed on paper substrates for creation of dual light responsive patterns.

(4) An advanced anti-counterfeiting technique was developed by printing a complex quick-response (QR) code using the dual-mode

fluorescent DJMT ink and single-mode fluorescent UCMP ink, which is more complicated and have great potential in high level of anti-counterfeiting applications.

References

[1] YAO Wei-jing, TIAN Qing-yong, WU Wei. Tunable emissions of upconversion fluorescence for security applications [J]. Advanced Optical Materials, 2019, 7: 1801171.

[2] HAN S, BAE H J, KIM J, SHIN S, CHOI S E, LEE S H, KWON S, PARK W. Lithographically encoded polymer microtaggant using high-capacity and error-correctable QR code for anti-counterfeiting of drugs [J]. Advanced Materials, 2012, 24: 5924−5929.

[3] YOON B, LEE J, PARK I S, JEON S, LEE J, KIM J M. Recent functional material based approaches to prevent and detect counterfeiting [J]. Journal of Materials Chemistry C, 2013, 1: 2388−2403.

[4] TAN Hai-hu, GONG Guo, XIE Shao-wen, SONG Ya, ZHANG Chang-fan, LI Na, ZHANG Dong, XU Li-jian, XU Jian-xiong, ZHENG Jie. Upconversion nanoparticles@ carbon dots@Meso-SiO_2 sandwiched core−shell nanohybrids with tunable dual-mode luminescence for 3D anti-counterfeiting barcodes [J]. Langmuir, 2019, 35: 11503−11511.

[5] GONG Guo, SONG Ya, TAN Hai-hu, XIE Shao-wen, ZHANG Chang-fan, XU Li-jian, XU Jian-xiong, ZHENG Jie. Design of core/active-shell $NaYF_4:Ln^{3+}@NaYF_4:Yb^{3+}$ nanophosphors with enhanced red−green−blue upconversion luminescence for anti-counterfeiting printing [J]. Composites Part B: Engineering, 2019, 179: 107504.

[6] SINGH R, SINGH E, NALWA H S. Inkjet printed nanomaterial based flexible radio frequency identification (RFID) tag sensors for the internet of nano things [J]. RSC Advances, 2017, 7: 48597−48630.

[7] LEE I H, LI G, LEE B Y, KIM S U, LEE B, OH S H, LEE S D. Selective photonic printing based on anisotropic Fabry−Perot resonators for dual-image holography and anti-counterfeiting [J]. Optics Express, 2019, 27: 24512−24523.

[8] ZHANG Ting, FU Liu-wa, CHEN Zhi-kang, CUI Yan-yan, LIU Xiao-xuan. Photochromic properties of spiropyran in epoxy resin as anti-counterfeiting coating on flexible materials [J]. Progress in Organic Coatings, 2016, 100: 100−104.

[9] KUMAR P, SINGH S, GUPTA B K. Future prospects of luminescent nanomaterial based security inks: From synthesis to anti-counterfeiting applications [J]. Nanoscale, 2016, 8: 14297−14340.

[10] ANDRES J, HERSCH R D, MOSER J E, CHAUVIN A S. A new anti-counterfeiting feature relying on invisible luminescent full color images printed with lanthanide-based inks [J]. Advanced Functional Materials, 2014, 24: 5029−5036.

[11] da LUZ L L, MILANI R, FELIX J F, RIBEIRO I R B, TALHAVINI M, NETO B A D, CHOJNACKI J, RODRIGUES M O, JÚNIOR S A. Inkjet printing of lanthanide-organic frameworks for anti-counterfeiting applications [J]. ACS Applied Materials & Interfaces, 2015, 7: 27115−27123.

[12] JIANG Kai, ZHANG Ling, LU Jun-feng, XU Chun-xiang, CAI Cong-zhong, LIN Heng-wei. Triple-mode emission of carbon dots: Applications for advanced anti-counterfeiting [J]. Angewandte Chemie International Edition, 2016, 55: 7231−7235.

[13] SANDHYARANI A, KOKILA M K, DARSHAN G P, BASAVARAJ R B, DARUKA PRASAD B, SHARMA S C, LAKSHMI T K S, NAGABHUSHANA H. Versatile core–shell $SiO_2@SrTiO_3:Eu^{3+},Li^+$ nanopowders as fluorescent label for the visualization of latent fingerprints and anti-counterfeiting applications [J]. Chemical Engineering Journal, 2017, 327: 1135−1150.

[14] BAI Li-qian, XUE Ning, ZHAO Yu-fei, WANG Xin-rui, LU Chao, SHI Wen-ying. Dual-mode emission of single-layered graphene quantum dots in confined nanospace: Anti-counterfeiting and sensor applications [J]. Nano Research, 2018, 11: 2034−2045.

[15] XIONG Qing-xia, XU Chao, JIAO Nian-ming, MA Xiang, ZHANG Yan-qiang, ZHANG Suo-jiang. Pure organic room-temperature phosphorescent *N*-allylquinolinium salts as anti-counterfeiting materials [J]. Chinese Chemical Letters, 2019, 30: 1387−1389.

[16] LIU Jian-bin, ZHUANG Yi-xi, WANG Li, ZHOU Tian-liang, HIROSAKI N, XIE Rong-jun. Achieving multicolor long-lived luminescence in dye-encapsulated meta-organic frameworks and its application to anticounterfeiting stamps [J]. ACS Applied Materials & Interfaces, 2018, 10: 1802−1809.

[17] SUN Li-wei, SHI Han-qiao, LI Wan-nan, XIAO Hong-mei, FU Shao-yun, CAO Xing-zhong, LI Zhuo-xin.. Lanthanum-doped ZnO quantum dots with greatly enhanced fluorescent quantum yield [J]. Journal of Materials Chemistry, 2012, 22: 8221−8227.

[18] KALYTCHUK S, WANG Y, POLÁKOVÁ K, ZBOŘIL R. Carbon dot fluorescence-lifetime-encoded anti-counterfeiting [J]. ACS Applied Materials & Interfaces, 2018, 10: 29902−29908.

[19] BAKHSHESHI-RAD H, DAYAGHI E, ISMAIL A, AZIZ M, AKHAVAN-FARID A, CHEN Xiong-biao. Synthesis and in-vitro characterization of biodegradable porous magnesium-based scaffolds containing silver for bone tissue engineering [J]. Transactions of Nonferrous Metals Society of China, 2019, 29: 984−996.

[20] DONG Hao, SUN Ling-dong, YAN Chun-hua. Energy transfer in lanthanide upconversion studies for extended optical applications [J]. Chemical Society Reviews, 2015, 44: 1608−1634.

[21] LIU Xiao-wang, WANG Yu, LI Xi-yan, YI Zhi-gao, DENG Ren-ren, LIANG Liang-liang, XIE, Xiao-ji, LOONG D T B, SONG Shu-yan, FAN Dian-yuan, ALL A H, ZHANG Hong-jie, HUANG Ling, LIU Xiao-gang. Binary temporal upconversion codes of Mn^{2+}-activated nanoparticles for multilevel anti-counterfeiting [J]. Nature Communications, 2017, 8: 899.

[22] XU Jian-xiong, FENG Ya-hui, WU Yan-xian, LI Yan-jun, OUYANG M, ZHANG Xi-ping, WANG Yong, WANG

Yang-yun, XU Li-jian. Noninvasive monitoring of bone regeneration using $NaYF_4$:Yb^{3+},Er^{3+} upconversion hollow microtubes supporting PLGA-PEG-PLGA hydrogel [J]. Reactive and Functional Polymers, 2019, 143: 104333.

[23] LI Li, CAO Xue-qin, ZHANG You, GUO Chang-xin. Synthesis and upconversion luminescence of Lu_2O_3: Yb^{3+},Tm^{3+} nanocrystals [J]. Transactions of Nonferrous Metals Society of China, 2012, 22: 373−379.

[24] HAN Ying-dong, LI Hong-yu, WANG Yang-bo, PAN Yue, HUANG Ling, SONG Feng, HUANG Wei. Upconversion modulation through pulsed laser excitation for anti-counterfeiting [J]. Scientific Reports, 2017, 7: 1320.

[25] YAO Wei-jing, TIAN Qing-yong, LIU Jun, XUE Qing-wen, LI Meng-xiao, LIU Li, LU Qiang, WU Wei. Preparation and RGB upconversion optic properties of transparent anti-counterfeiting films [J]. Nanoscale, 2017, 9: 15982−15989.

[26] YOU Min-li, LIN Min, WANG Shu-rui, WANG Xue-min, ZHANG Ge, HONG Yuan, DONG Yu-qing, JIN Guo-rui, XU Feng. Three-dimensional quick response code based on inkjet printing of upconversion fluorescent nanoparticles for drug anti-counterfeiting [J]. Nanoscale, 2016, 8: 10096−10104.

[27] CHEN Lei, WEI Xian-hua, FU Xu. Effect of Er substituting sites on upconversion luminescence of Er^{3+}-doped $BaTiO_3$ films [J]. Transactions of Nonferrous Metals Society of China, 2012, 22: 1156−1160.

[28] KUMAR P, DWIVEDI J, GUPTA B K. Highly luminescent dual mode rare-earth nanorod assisted multi-stage excitable security ink for anti-counterfeiting applications [J]. Journal of Materials Chemistry C, 2014, 2: 10468−10475.

[29] SUN Tian-ying, XU Bing-zhe, CHEN Bing, CHEN Xian, LI Ming-yu, SHI Peng, WANG Feng. Anti-counterfeiting patterns encrypted with multi-mode luminescent nanotaggants [J]. Nanoscale, 2017, 9: 2701−2705.

[30] LIU Rui, TU Da-tao, LIU Yong-sheng, ZHU Hao-miao, LI Ren-fu, ZHENG Wei, MA En, CHEN Xue-yuan. Controlled synthesis and optical spectroscopy of lanthanide-doped $KLaF_4$ nanocrystals [J]. Nanoscale, 2012, 4: 4485−4491.

[31] HUANG Qing-ming, YU Han, ZHANG Xin-qi, CAO Wen-bing, YU Jian-chang. Upconversion performance enhancement of $NaYF_4$:Yb/Tm by codoping Hf^{4+} as energy migrator [J]. Acta Chimica Sinica, 2016, 74: 191−198.

[32] ZHOU Bo, TAO Li-li, CHAI Yang, LAU S P, ZHANG Qing-yuan, TSANG Y H. Constructing interfacial energy transfer for photon up- and down-conversion from lanthanides in a core-shell nanostructure [J]. Angewandte Chemie International Edition, 2016, 55: 12356−12360.

[33] CHEN Liang-jian, CHEN Tian, CAO Jun, LIU Bei-lei. Effect of Tb/Mg doping on composition and physical properties of hydroxyapatite nanoparticles for gene vector application [J]. Transactions of Nonferrous Metals Society of China, 2018, 28: 125−136.

[34] YAO Wei-jing, TIAN Qing-yong, LIU Jun, WU Zhao-hui, CUI Shu-yuan, DING Jin, DAI Zhi-gao, WU Wei. Large-scale synthesis and screen printing of upconversion hexagonal-phase $NaYF_4$:Yb^{3+},Tm^{3+}/Er^{3+}/Eu^{3+} plates for security applications [J]. Journal of Materials Chemistry C, 2016, 4: 6327−6335.

[35] YOU Min-li, ZHONG Jun-jie, HONG Yuan, DUAN Zhen-feng, LIN Min, XU Feng. Inkjet printing of upconversion nanoparticles for anti-counterfeit applications [J]. Nanoscale, 2015, 7: 4423−4431.

[36] LIU Yan-lan, AI Ke-long, LU Le-hui. Designing lanthanide-doped nanocrystals with both up- and down-conversion luminescence for anti-counterfeiting [J]. Nanoscale, 2011, 3: 4804−4810.

[37] KUMAR P, SINGH S, GUPTA B K. A novel approach to synthesise a dual-mode luminescent composite pigment for uncloneable high-security codes to combat counterfeiting [J]. Chemistry−A European Journal, 2017, 23: 17144−17151.

[38] LI Meng-xiao, YAO Wei-jing, LIU Jun, TIAN Qing-yong, LIU Li, DING Jin, XUE Qing-wen, LU Qiang, WU Wei. Facile synthesis and screen printing of dual-mode luminescent $NaYF_4$:Er,Yb(Tm)/carbon dots for anti-counterfeiting applications [J]. Journal of Materials Chemistry C, 2017, 5: 6512−6520.

[39] LIU Yang, ZHANG Ming, YIN Xin-feng, HUANG Zhou, WANG Lei. Debonding detection of reinforced concrete (RC) beam with nearsurface mounted (NSM) prestressed carbon fiber reinforced polymer (CFRP) plates using embedded piezoceramic smart aggregates (SAs) [J]. Applied Sciences, 2020, 10: 50.

[40] LI Rui-min, ZHANG Yu-ting, TAN Jing, WAN Jia-xun, GUO Jia, WANG Chang-chun. Dual-mode encoded magnetic composite microsphere based on fluorescence reporters and Raman probes as covert tag for anticounterfeiting applications [J]. ACS Applied Materials & Interfaces, 2016, 8: 9384−9394.

[41] LEI Lei, DAI Xiao-rui, CHENG Yao, WANG Yuan-sheng, XIAO Zhen, XU Shi-qing. Dual-mode color tuning based on upconversion core/triple-shell nanostructure [J]. Journal of Materials Chemistry C, 2019, 7: 3342−3350.

[42] CHEN Xian, PENG Den-feng, JU Qiang, WANG Feng. Photon upconversion in core−shell nanoparticles [J]. Chemical Society Reviews, 2015, 44: 1318−1330.

[43] LIU Yong-sheng, TU Da-tao, ZHU Hao-miao, LI Ren-fu, LUO Wen-qin, CHEN Xue-yuan. A strategy to achieve efficient dual-mode luminescence of Eu^{3+} in lanthanides doped multifunctional $NaGdF_4$ nanocrystals [J]. Advanced Materials, 2010, 22: 3266−3271.

[44] DING Ming-ye, CHEN Da-qin, WAN Zhong-yi, ZHOU Yang, ZHONG Jia-song, XI Jun-hua, JI Zhen-guo. Achieving efficient Tb^{3+} dual-mode luminescence via Gd-sublattice-mediated energy migration in a $NaGdF_4$ core−shell nanoarchitecture [J]. Journal of Materials Chemistry C, 2015, 3: 5372−5376.

[45] XIE Shao-wen, GONG Guo, SONG Ya, TAN Hai-hu, ZHANG Chang-fan, LI Na, ZHANG Yan-xian, XU Li-jian, XU Jian-xiong, ZHENG Jie. Design of novel lanthanide-doped core-shell nanocrystals with dual up-conversion and down-conversion luminescence for anti-counterfeiting printing [J]. Dalton Transactions, 2019, 48: 6971−6983.

[46] YIN Xin-feng, SONG Gang-bing, LIU Yang. Vibration suppression of wind/traffic/bridge coupled system using multiple pounding tuned mass dampers (MPTMD) [J]. Sensors, 2019, 19: 1133.

[47] WANG Ling-xiao, GUO Shuang-li, LIU Dong-mei, HE Ji-jun, ZHOU Jie, ZHANG Kun, WEI Yang, PAN Yue, GAO Chao, YUAN Ze, LEI Dang-yuan, XIE Xiao-ji, HUANG Ling. Plasmon-enhanced blue upconversion luminescence by indium nanocrystals [J]. Advanced Functional Materials, 2019, 29: 1901242.

[48] HOMANN C, KRUKEWITT L, FRENZEL F, GRAUEL B, WÜRTH C, RESCH-GENGER U, HAASE M. $NaYF_4$:Yb, Er/$NaYF_4$ core/shell nanocrystals with high upconversion luminescence quantum yield [J]. Angewandte Chemie International Edition, 2018, 57: 8765−8769.

[49] PHUONG H T, HUONG T T, VINH L T, KHUYEN H T, THAO D T, HUONG N T, LIEN P T, MINH L Q. Synthesis and characterization of $NaYF_4:Yb^{3+},Er^{3+}$@silica—N═folic acid nanocomplex for bioimaginable detecting MCF-7 breast cancer cells [J]. Journal of Rare Earths, 2019, 37: 1183−1187.

[50] XIE Shao-wen, TONG Chao, TAN Hai-hu, LI Na, GONG Liang, XU Jian-xiong, XU Li-jian, ZHANG Chang-fan. Hydrothermal synthesis and inkjet printing of hexagonal-phase $NaYF_4:Ln^{3+}$ upconversion hollow microtubes for smart anti-counterfeiting encryption [J]. Materials Chemistry Frontiers, 2018, 2: 1997−2005.

[51] LI Dan, MA Qian-li, XI Xue, DONG Xiang-ting, YU Wen-sheng, WANG Jin-xian, LIU Gui-xia. Dy^{3+} and Eu^{3+} Co-doped $NaGdF_4$ nanofibers endowed with bifunctionality of tunable multicolor luminescence and paramagnetic properties [J]. Chemical Engineering Journal, 2017, 309: 230−239.

[52] DU Guo, SONG Ya, LI Na, XU Li-jian, TONG Chao, FENG Ya-hui, CHEN Tie-hong, XU Jian-xiong. Cage-like hierarchically mesoporous hollow silica microspheres templated by mesomorphous polyelectrolyte-surfactant complexes for noble metal nanoparticles immobilization [J]. Colloids and Surfaces A: Physicochemical and Engineering Aspects, 2019, 575: 129−139.

[53] HUANG Qi-ying, YE Wei-hao, JIAO Xian-fu, YU Lin-liang, LIU Ying-liang. Efficient upconversion fluorescence in $NaYF_4:Yb^{3+},Er^{3+}$/m$NaYF_4$ multilayer core−shell nanoparticles [J]. Journal of Alloys and Compounds, 2018, 763: 216−222.

[54] SHRIVASTAVA N, ROCHA U, MURACA D, SILVA W, JACINTO C, KUMAR R, SHARMA S K. Insight into dual-modality of triply doped magnetic-luminescent iron-oxide/$NaGdF_4:RE^{3+}$ (RE = Ce, Tb, Dy) nanoparticles [J]. Materials Letters, 2018, 213: 358−361.

具有套管结构 $NaYF_4:Yb^{3+},Tm^{3+}$@$NaGdF_4:Ce^{3+},Eu^{3+}$晶体的制备及在双模式荧光防伪中的应用

陈殷[1]，谢少文[1]，童超[1]，谭海湖[1]，许利剑[1]，李娜[1,2]，许建雄[1]

1. 湖南工业大学 生命科学与化学学院 生物医用纳米材料与器件湖南省重点实验室，株洲 412007；
2. 湖南工业大学 冶金与材料工程学院 电化学绿色冶金技术湖南省高等学校重点实验室，株洲 412007

摘　要：通过聚丙烯酸(PAA)调介的水热法在 $NaYF_4:Yb^{3+},Tm^{3+}$微管上外延生长 $NaGdF_4:Ce^{3+},Eu^{3+}$壳层，制备新型亲水性 $NaYF_4:Yb^{3+},Tm^{3+}$@$NaGdF_4:Ce^{3+},Eu^{3+}$双模式荧光套管(DJMT)。研究表明，PAA 配体在 $NaYF_4:Yb^{3+},Tm^{3+}$微管表面形成 $NaGdF_4:Ce^{3+},Eu^{3+}$壳层中起到重要的结构导向作用。$NaYF_4:Yb^{3+},Tm^{3+}$@$NaGdF_4:Ce^{3+},Eu^{3+}$双模式荧光双夹层微管的生长经历由 β-$NaGdF_4$ 和 β-$NaYF_4$ 两相混合物到 β-$NaYF_4$@$NaGdF_4$ 复合晶体的晶相转变过程，同时，颗粒形貌由 β-$NaGdF_4:Ce^{3+},Eu^{3+}$纳米棒与 β-$NaYF_4:Yb^{3+},Tm^{3+}$微管的混合物演变为 $NaYF_4:Yb^{3+},Tm^{3+}$@$NaGdF_4:Ce^{3+},Eu^{3+}$套管结构。DJMTs 的生长机理遵循 Ostwald 熟化机制，生长过程中原位生成的 β-$NaGdF_4:Ce^{3+},Eu^{3+}$纳米棒经过溶解−再成核以及表面沉积等过程，在 $NaYF_4:Yb^{3+},Tm^{3+}$微管的表面附着 β-$NaGdF_4:Ce^{3+},Eu^{3+}$壳层。制备的 DJMT 具有蓝色上转换和红色下转换荧光特性，可制成环保的荧光油墨，通过喷墨打印实现高度安全的荧光防伪图案的输出。

关键词：稀土掺杂氟化物；核壳结构；双模式荧光；喷墨打印；防伪

(Edited by Bing YANG)